THE ARCHIVE OF MECHANICAL ENGINEERING

Vol. LII 2005 Number 2

Key words: *helicopter, rotor, neural network*

JAROSŁAW STANISŁAWSKI[*)]

APPLICATION OF NEURAL NETWORK TO DETECTING FAULTS OF HELICOPTER ROTOR

The paper presents the possibilities of neural network application in recognition of rotor blade faults. Computer calculated data of rotor response due to faults were used for neural network training. The rotor was modeled by elastic axes with distribution of lumped masses. The rotor defects were simulated by changing aerodynamic, inertial or stiffness properties of one of the blades. Time results were subjected to spectral analysis for the purpose of neural networks training.

1. Introduction

Flight safety is one of the main demands of helicopter users. During life-time of exploitation, the helicopter structure can be damaged due to varying loads. In flight conditions, the main rotor is subjected to complex system of vibratory aerodynamic and inertial forces depending on flight speed, rotor speed and control of blade pitching angle. The use of trained neural networks can help in recognition of rotor blades failures. For the network training purpose, it is necessary to collect data connecting the level of damage with other measurable parameters.

The research works on using artificial neural networks were conducted in respect to helicopters utilizing recorded flight data [1] to foresee load level of the main rotor in manoeuvres. The difficulties in gathering the measurement data for real objects with damaged structural parts prompt us to use simulation methods. Rotor models based on finite element method were used for load calculation including effects of simulated blade faults [2], [3]. The obtained

[*)] *Institute of Aviation, Al.Krakowska 110/114, 02-256 Warsaw, Poland; E-mail: stanjar@ilot.edu.pl*

results formed the data for training neural networks detecting the rotor damages.

In this paper, the author presents the possibilities of neural networks in recognizing the rotor failures for flight conditions covering hover and forward speed. The results of calculation, including blade, hub and shaft loads and blade motion parameters, were used to train neural networks. The simulation calculations for a rotor with damaged blade were conducted using computer program code generated at the Institute of Aviation [4], [5].

2. Model of main rotor

The physical model of rotor consists of the elastic axes replacing the real blades (Fig. 1).

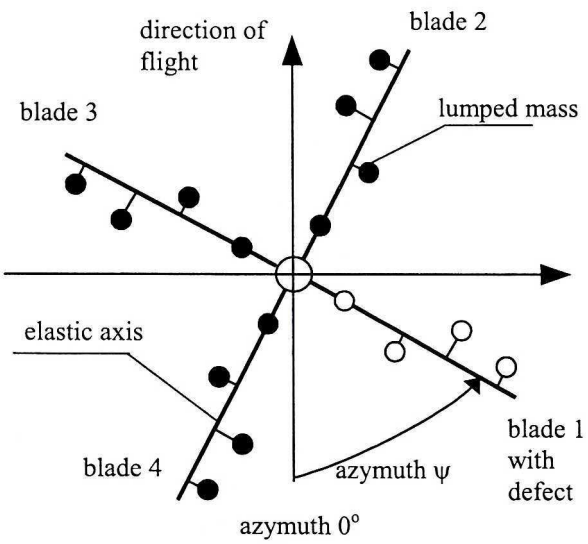

Fig. 1. Rotor scheme with defected blade

The elastic axis of each blade can be bent in the flapping plane, in the lagging plane and can be twisted. The elastic axis includes also the arm of rotor hub, which is settled on stiffness shaft. It was assumed that in undeformed state the elastic axis coincided with the pitching axis of each blade. The real blade mass distribution was replaced by lumped masses connected with the elastic axis. Blade stiffness properties were assigned to segments of axis located between sections with lumped masses. Besides elastic deflections, the blade elements undergo displacements subsequent to collective and cyclic control.

The equations of blade motion form a mathematical model of the rotor. For the elastic axis, the equation of motion can be derived using Lagrange formula:

$$\frac{d}{dt}\left(\frac{\partial T}{\partial \dot{q}_i}\right) - \frac{\partial T}{\partial q_i} + \frac{\partial U}{\partial q_i} = Q_i \quad i = 1, ..., n \tag{1}$$

The potential energy of elastic axis being bent and twisted equals:

$$U = \int_0^R \frac{M_Y^2}{2EJ_Y} dx + \int_0^R \frac{M_Z^2}{2EJ_Z} dx + \int_0^R \frac{M_S^2}{2GJ_X} dx \tag{2}$$

The kinetic energy of elastic axis equals:

$$T = \frac{1}{2}\int_0^R m(x)V_Y^2(x)dx + \frac{1}{2}\int_0^R m(x)V_Z^2(x)dx + \frac{1}{2}\int_0^R I_X(x)\Omega_\varphi^2(x)dx \tag{3}$$

The bending and twisting moment loading that loads the elastic axis can be expressed according to deformations: deflection in the plane of rotation y, deflection out of-plane z and angle of torsion φ:

$$M_Y = EJ_Y\frac{d^2z}{dx^2}, \quad M_Z = EJ_Z\frac{d^2y}{dx^2}, \quad M_S = GJ_X\frac{d\varphi}{dx}. \tag{4}$$

In the case of whirling blade, the stiffening effects of centrifugal forces must be considered in the equations of motion. The centrifugal forces per unit length that reduce bending moments out of plane are equal:

$$p_Z = \frac{d}{dx}\left(N\frac{dz}{dx}\right) \tag{5}$$

and in plane:

$$p_y = \frac{d}{dx}\left(N\frac{dy}{dx}\right) - m(x)\,\omega^2 y \tag{6}$$

where

$$N = \int_0^R m(x)\,\omega^2 x\,dx \tag{7}$$

centrifugal force for cross-section in distance r from axis of rotor shaft.

Substituting Eqs.(2)÷(7) into Eqs. (1) yields the equations of blade motion in the following form:
for bending in-plane

$$\int_0^R m(x)\ddot{y}dx + \int_0^R \left\{\frac{d^2}{dx^2}\left[EJ_z\left(\frac{d^2y}{dx^2}\right)\right] - p_y\right\}dx = \int_0^R (F_{YE} - F_{YI})dx \tag{8}$$

for bending out-of-plane

$$\int_0^R m(x)\ddot{z}dx + \int_0^R \left\{\frac{d^2}{dx^2}\left[EJ_y\left(\frac{d^2z}{dx^2}\right)\right] - p_z\right\}dx = \int_0^R (F_{ZE} - F_{ZI})dx \tag{9}$$

and for torsion

$$\int_0^R I_x(x)\ddot{\varphi}dx + \int_0^R \frac{d}{dx}\left[GJ_x\left(\frac{d\varphi}{dx}\right)\right]dx = \int_0^R (M_{SE} - M_{SI})dx \tag{10}$$

where F_{YE}, F_{ZE}, M_{SE} – shearing forces and torsion moment of external blade loading, F_{YI}, F_{ZI}, M_{SI} – inertial forces and moment without components $m\ddot{y}$, $m\ddot{z}$, $I_x\ddot{\varphi}$

A Galerkin procedure is used to obtain the solution to Eqs. (8)÷(10). In this case, the deformation of elastic axis y, z, φ are assumed as a superposition of modal solution ρ_{i1}, δ_{i2}, η_{i3} of the form:

$$y(x,t) = \sum_{i1=1}^{I1} \rho_{i1}(t)\, y_{i1}(x), \tag{11}$$

$$z(x,t) = \sum_{i2=1}^{I2} \delta_{i2}(t)\, z_{i2}(x), \tag{12}$$

$$\varphi(x,t) = \sum_{i3=1}^{I3} \eta_{i3}(t)\, \varphi_{i3}(x) \tag{13}$$

where y_{i1}, z_{i2}, φ_{i3} are blade eigen modes for in-plane bending, out-of-plane bending and torsion respectively; $I1$, $I2$, $I3$ are number of eigen modes for bending and torsion.

Taking into consideration Eqs. (11)÷(13), one can transform the blade motion equation (8)÷(10) to a set of differential equations:

$$\ddot{\rho}_{i1} + \rho_{i1} p_{i1}^2 = Q_{Y_{i1}}, \quad i1 = 1, ..., I1$$

$$\ddot{\delta}_{i2} + \delta_{i2} f_{i2}^2 = Q_{Z_{i2}}, \quad i2 = 1, ..., I2 \tag{14}$$

$$\ddot{\eta}_{i3} + \eta_{i3} v_{i3}^2 = Q_{\varphi_{i3}}, \quad i3 = 1, ..., I3$$

where p, f, v are eigen frequencies of the considered modes, and $Q_{Y_{i1}}, Q_{Z_{i2}}, Q_{\varphi_{i3}}$ are generalized forces. The Runge-Kutta algorithm is used to solve the set of equation (14). Integrating the distribution of forces along the blades makes it possible to calculate loads of rotor hub and shaft.

Aerodynamic sectional forces and moments are calculated using Tarzanin dynamic stall model [6]. For blade element, the local angle of attack α depends on temporary airflow terms:

$$\alpha = \varphi - arc\,\mathrm{tg}\left(\frac{v_Z}{v_X}\right) \tag{15}$$

v_x, v_z – components of airflow, φ – pitch angle of blade element

$$\varphi = \varphi_0 + \varphi_x \cos \omega t + \varphi_y \sin \omega t + \varphi_s - \kappa\beta \tag{16}$$

where: φ_0 – collective pitch control angle,
φ_x, φ_y – lateral and longitudinal cyclic control angle, φ_s – local torsion angle,
κ – flap and pitch coefficient, β – flapping angle.

3. Simulation of rotor defects

The calculations, made for four blades rotor of medium weight helicopter, were conducted to collect data useful for neural network training. The level flight conditions with speed range from hover up to V = 250 km/h were considered. The rotor defects were simulated only for one blade by changing its aerodynamic, inertial or stiffness properties. The others blades remained identical with their properties unchanged.
The following faults, denoted as (D1)-(D6), were selected:

- blade mass increase as a result of moisture absorption with uniform distribution along the blade up to 1% of total blade mass (D1);
- misadjusted pitch link with 1° difference of pitch angle to other blades (D2);

- fault of improper trim tab angle changing the aerodynamic characteristics of blade section with the tab (D3):
  - increase of drag coefficient $\Delta c_x = 0.003$,
  - increase of maximum lift coefficient $\Delta c_z = 0.05$,
  - change of moment coefficient $\Delta c_{mo} = -0.01$,
  - increase of derivative lift coefficient to attack angle $\Delta(dc_z/d\alpha) = 0.05$ (1/rd),
  - change of zero lift angle $\Delta\alpha = 1°$;
- damage of blade damper with total decay of lead-lag moment damping (D4);
- loss of trim mass at the tip blade $\Delta m = 0.1$ kg (D5);
- 10% stiffness decrease of blade pitch link (D6).

The mentioned values of faults or changes of blade properties were assumed as fully developed defects. For six kinds of defects, a mathematical model was used to predict time function of the rotor shaft forces and moments, hub arm bending moments, blade bending moments, deflection of blade tip, flap and lag angles and the moment of blade pitch control for the increasing percentage level of faults from 0% (no defect) to 100% (developed defect). One considered 11 values of speed flight, 6 defect kinds and 100 increasing defect levels what yielded 6611 cases for computing including 11 cases with no defect.

Examples of the obtained time functions for flight speed $V = 250$ km/h are shown in Fig. $2 \div 6$, where, due to constant rotor speed, time was replaced by azimuth position of blade number 1. Fig. 2 shows the comparison of thrust force for rotor without failure and for the case of incorrect (100%) pitch link adjustment for one blade.

The comparisons for rotor shaft torsion moment (Fig. 3), blade bending moment (Fig. 4), angle of flapping (Fig. 5) and blade pitch control moment (Fig. 6) also pertain to the cases of fully developed faults.

Time results were subjected to fast Fourier transformation to form vector of cosine and sine components of the selected harmonics for the purpose of neural network training.

For the parameters shown in Fig. $2 \div 6$, the influence of the developed faults on the harmonic amplitudes are presented in Fig. $7 \div 11$. The examples of blade parameters changes due to increasing level of defects or flight speed are shown in Fig. $12 \div 13$.

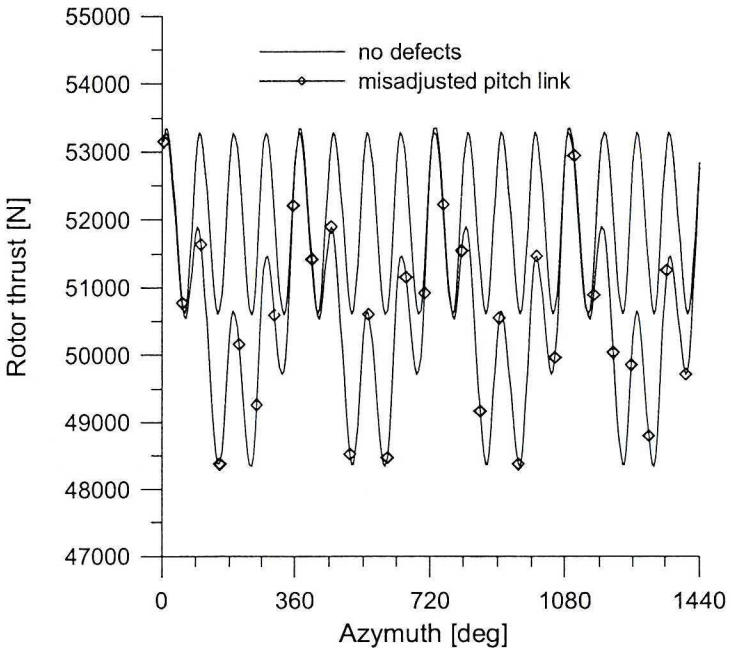

Fig. 2. Thrust of the four blades rotor for the level flight speed $V = 250$ km/h, comparison for rotor without faults and for rotor with misadjusted pitch link of one blade

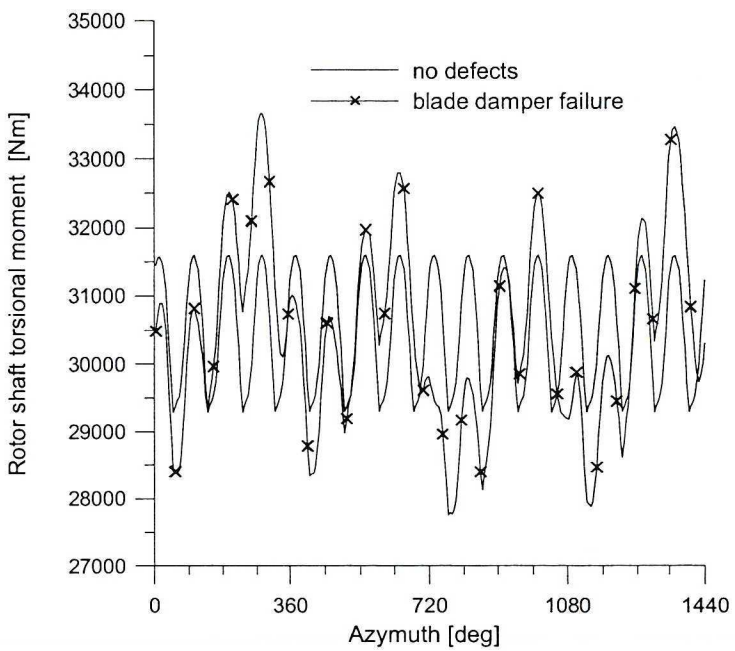

Fig. 3. Rotor shaft torsion moment for the level flight with speed $V = 250$ km/h, comparison between rotor without defects and rotor with failed one blade damper

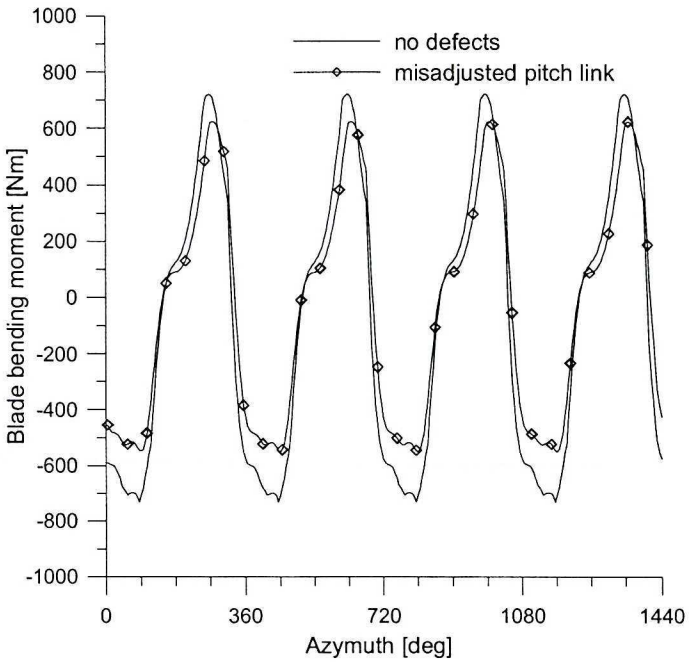

Fig. 4. Blade bending moment in plane of greater stiffness on radius $r = 0.42R$ for the level flight with speed $V = 250$ km/h, comparison between rotor without faults and rotor with misadjusted pitch link of one blade

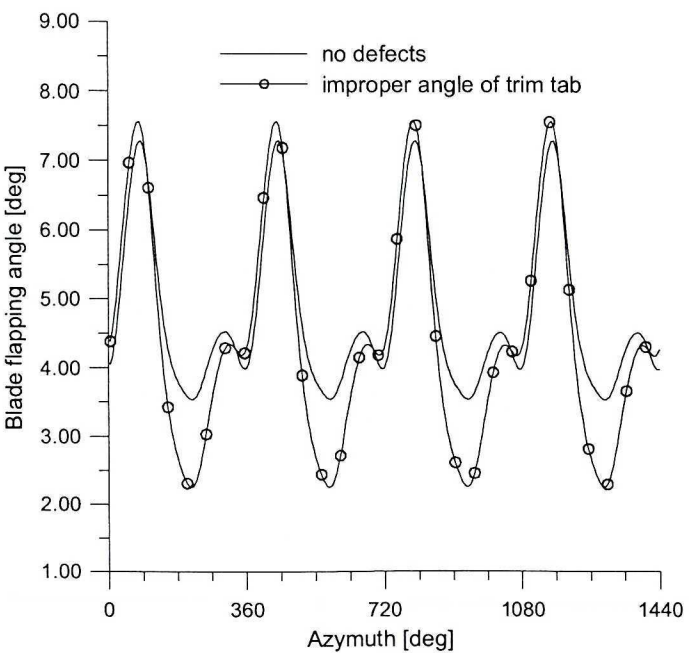

Fig. 5. Blade flapping angle for the level flight with speed $V = 250$ km/h, comparison between rotor without faults and one blade with improper trim tab angle

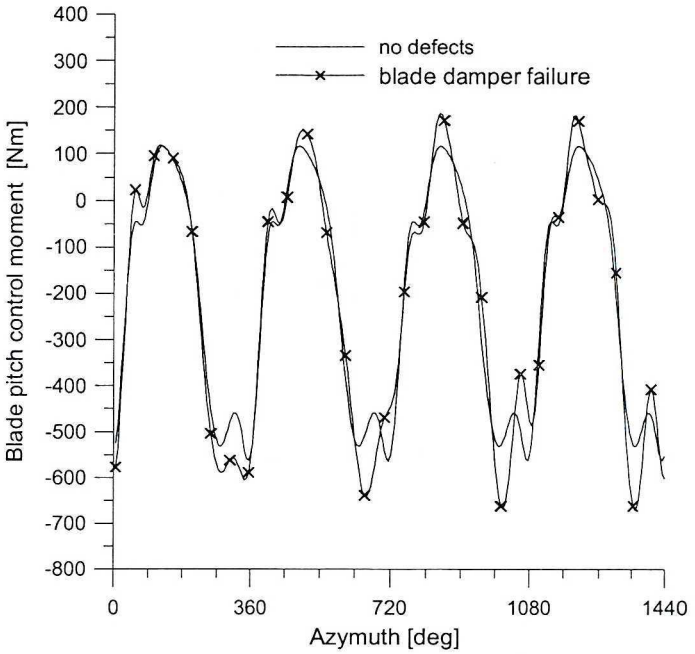

Fig. 6. Blade pitch control moment for the level flight with speed $V = 250$ km/h, comparison between rotor without defects and rotor with failed one blade damper

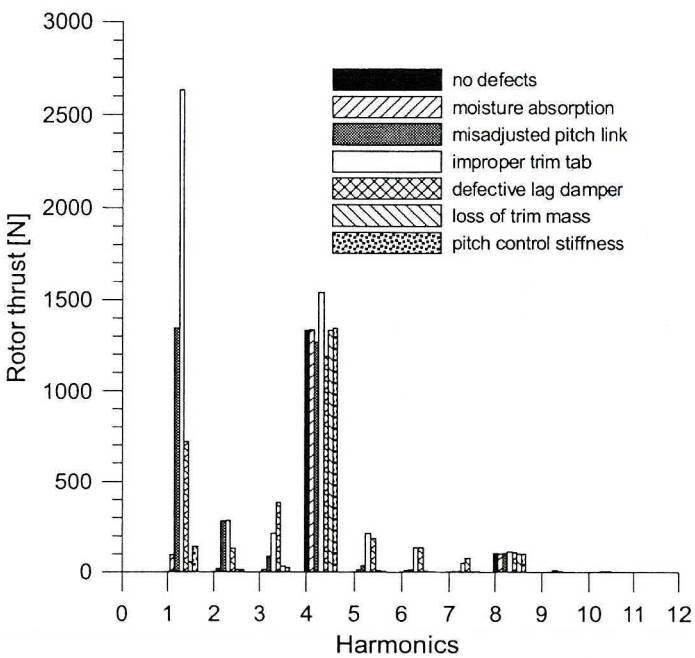

Fig. 7. Effects of developed faults on harmonic amplitudes of the rotor thrust for condition of flight with speed $V = 250$ km/h (constant component not shown)

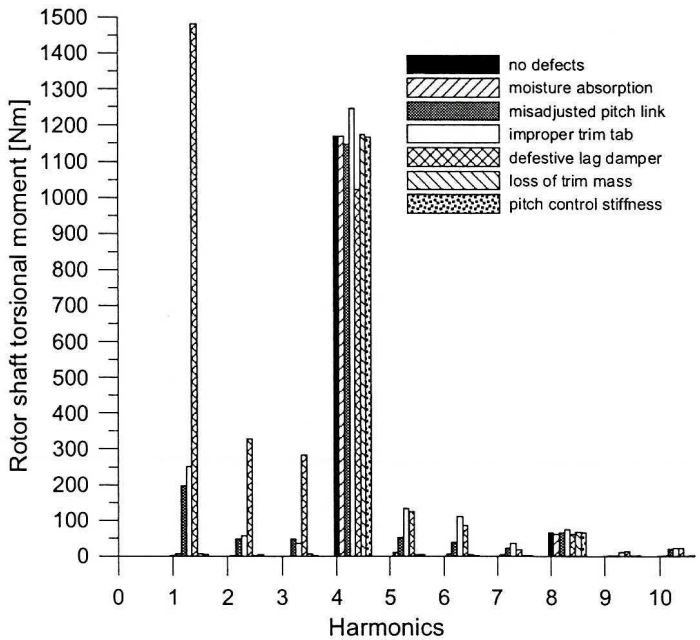

Fig. 8. Effects of developed faults on harmonic amplitudes of the rotor shaft torsion moment for condition of flight with speed $V = 250$ km/h (constant component not shown)

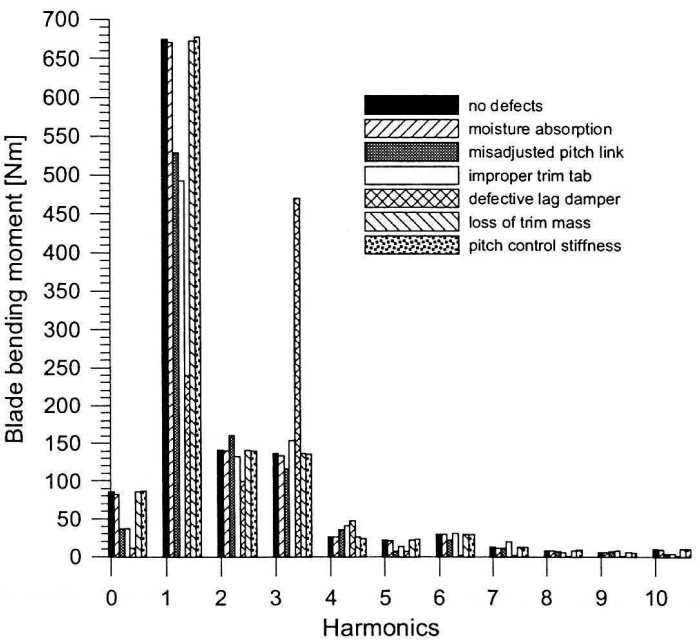

Fig. 9. Effects of developed faults on harmonic amplitudes of the blade bending moment in plane of higher stiffness on $r = 0.42R$ for condition of flight with speed $V = 250$ km/h

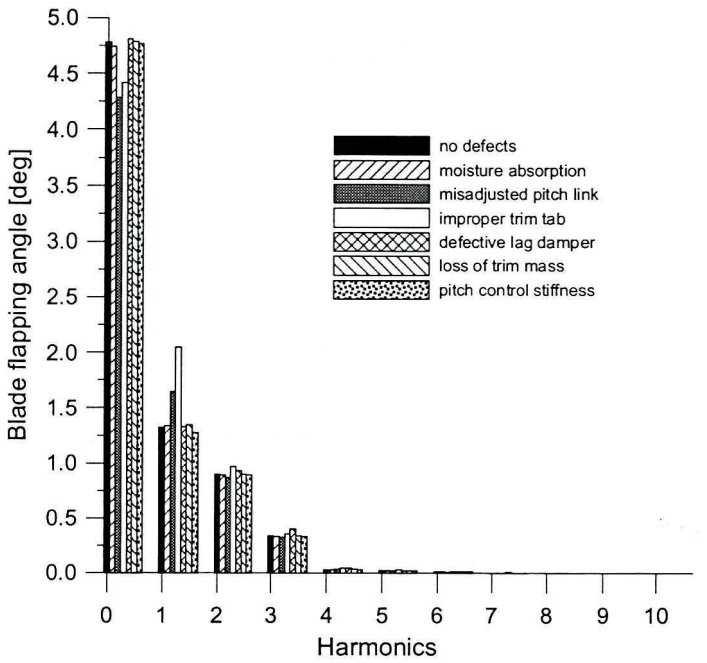

Fig. 10. Effects of developed faults on harmonic amplitudes of the blade flapping angle for condition of flight with speed $V = 250$ km/h

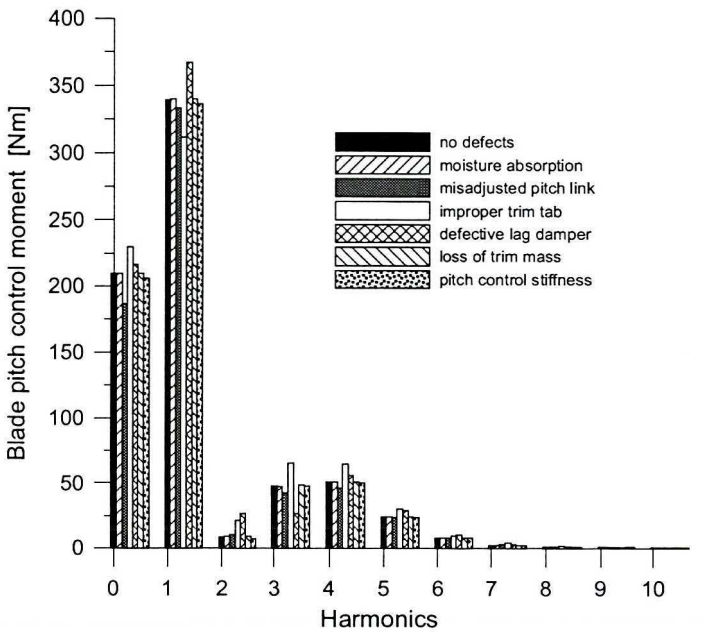

Fig. 11. Effects of developed faults on harmonic amplitudes of the blade pitch control moment for condition of flight with speed $V = 250$ km/h

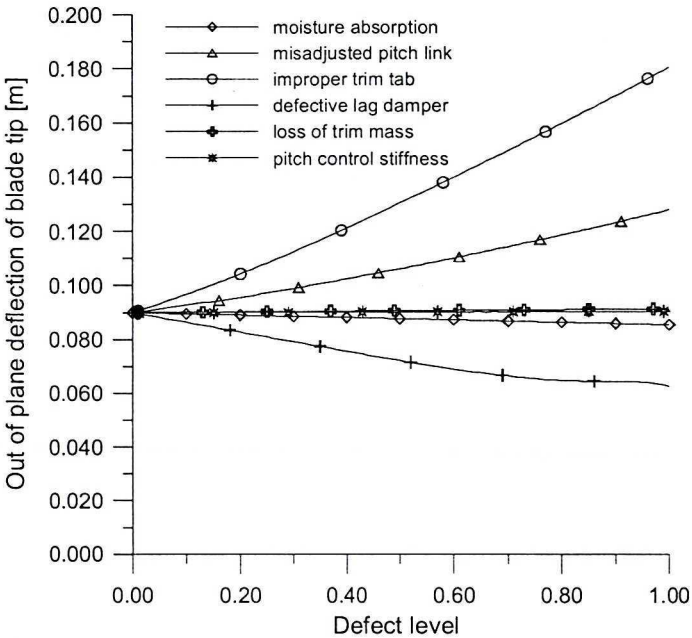

Fig. 12. Changes of first harmonics of blade tip deflection out of plane due to increasing defects for flight speed $V = 250$ km/h

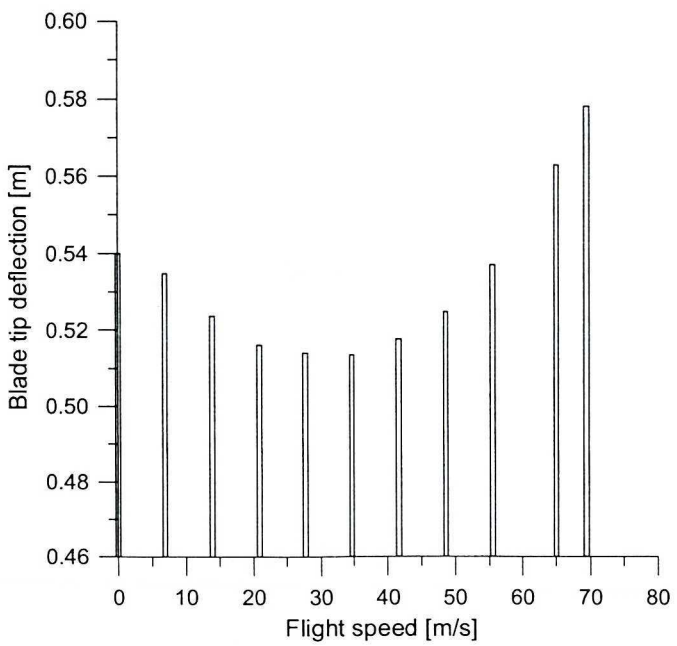

Fig. 13. Changes of constant component of blade tip deflection due to flight speed for fully misadjusted pitch link defect

Table 1.
Spectrum components at frequencies (related to rotor speed) initially selected to network training file

parameter	frequency
Loads of rotor shaft	0.0, 0.25, 0.5, 0.75, 1.0, 1.25, 1.75, 2.0, 2.25, 3.0, 3.25, 4.0, 4.25, 5.0, 5.25, 6.0 6.25, 7.0, 7.25, 8.0
Blade and hub arm parameters	0.0, 1.0, 2.0, 3.0, 3.25, 4.0, 4.25, 5.0

In the case of rotor with identical blades without defects, the spectrum of shaft loads includes harmonics of numbers equal to the multiple of blade number. The other harmonics vanish on the rotor hub. If the blade is damaged and its properties are different from the other ones than in the spectrum of rotor shaft loads there emerge additional harmonics with number not equal to the multiple of rotor blade number.

The file for initial neural network training includes harmonics of the following rotor shaft loads: rotor thrust, longitudinal and side forces, rolling and pitching moments and torsion moment. The data file also includes harmonics of hub arm in plane and out of plane bending moments and the following blade parameters: bending moments in the plane of low stiffness at location of *0.12R*, and *0.42R*; bending moments in the plane of higher stiffness at location of *0.12R*, *0.42R*, and *0.61R*; deflections in plane and out of plane and the torsion angle of blade tip; the flap angle, the lag angle and blade pitch control moment. The spectral analysis was conducted in a frequency range up to the 10^{th} harmonic of rotor speed with steps equal *0.25* frequency of rotor speed. The selected frequencies of spectrum components taken into consideration in training file are shown in Table 1. For each applied frequency the results of spectral analysis were put in the training file as the following pair of numbers:

$$F_1 = A\cos(n\omega t + \varphi),$$
$$F_2 = A\sin(n\omega t + \varphi),$$

where: A – amplitude, ω – rotor speed.

4. Results of neural network training

The STATISTICA Neural Network program with automatic network designer function was applied for network training. During training, it is possible to find a suitable network structure that gives output with a minimized error. Basic input data are divided into learning, validation and testing files. The learning file is used in the training process. In the cases of too

little data or too complicated structure of the network, an overtraining effect may occur what means too much fitting of the network structure to the learning data. The overtrained network is not adapted to other data and gives the output with larger error. Validation data, not taken for learning, are used to identify the overtraining effect. Testing data are used for final checking of the trained network. The results of learning depend on the number of parameters in data files and on the number of presented events. It is recommended to simplify the network by reducing the input data to the parameters of the highest influence on the correctness of network output.

The blade damage detecting was divided in two stages. The scheme of the proposed diagnostic system for recognition of the kinds of the blade faults in the first step, and estimation of the level of previously recognized defect in the second step, is shown in Fig. 14. In the first step, the network performs a classifying task. In the next step, for the recognized fault kind, the network with regression task – individual for each kind of fault – will estimate the level of development of rotor defect.

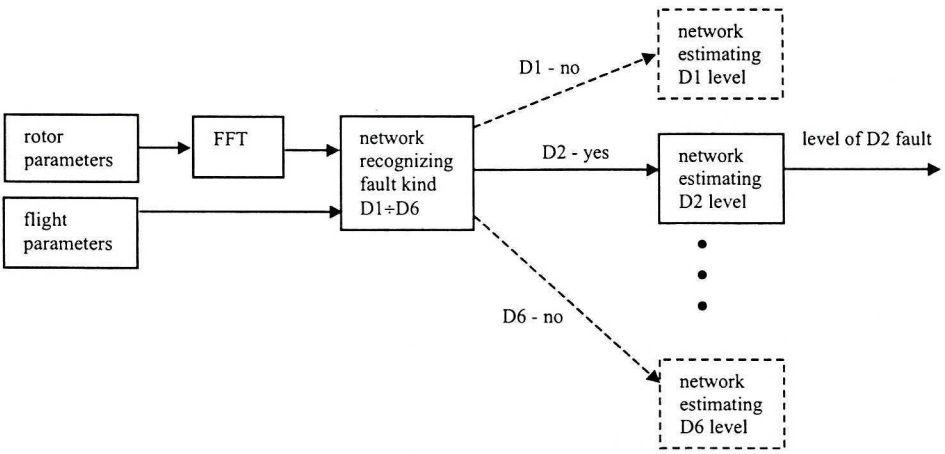

Fig. 14. Scheme of the diagnostic system for recognizing the kinds of blade faults and estimation of their levels

Input data file components for network designer function (see table 2) including rotor forces and blade tip deflection were selected after preliminary trainings. The neural network obtained in the training procedure was a feedforward multilayer perceptron with structural scheme (12:12-17-6:1) shown in Fig. 15. The input file of the network was reduced in comparison with the number of components for designer function (table 2). That network (12:12-17-6:1) was able to recognize kinds of blade defects in the flight speed range from hover up to V = 250km/h with network quality factor reaching the value of *0.988* for the

testing file part of input data cases. For the classifying network, the quality factor is defined as a proportion of the number of correctly recognized events to all presented events. The lack of flight speed between components of the network input file could be explained due to rotor longitudinal force changes, whose value depends exactly on helicopter speed in steady flight condition.

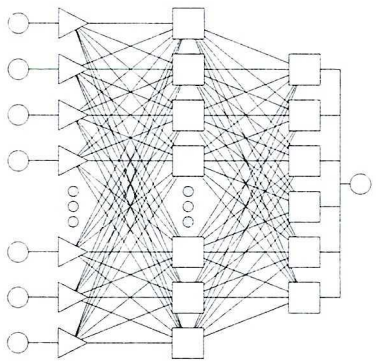

Fig. 15. The neural network scheme of structure (12:12-17-6:1) for recognition of the kinds of blade damage

Such parameters as rotor forces or blade tip deflection can be measured using special stand at wind tunnel examination, but they are difficult to measure in flight test conditions. Neural network input data for airborne application ought to be changed. The training file was corrected by including parameters that had weaker influence on network output but were measurable in flight tests. The corrected input file for designer function consist of the harmonics of blade bending moments, the rotor arm bending moments, the flapping and lagging angles and the pitch control moment (table 3). In the training procedure, the classifying network of feedforward multilayer perceptron type (27:27-21-6:1) was obtained. Neurons in the input layer had a linear function with saturation activation. Neurons in the hidden and output layer had a sigmoid activation function. The results of blade faults recognition for 6611 presented events are shown in tables $5 \div 7$. The neural network output was false for 284 events. The network quality factor decreased to *0.948* in the case of testing file (table 4). The incorrect recognition occurred only for the events at early stages of defect growing, and they did not exceed 18% of the assumed fully developed damage level.

Table 2.

Input for desiner function including rotor forces and input file for trained network (12:12-17-6:1) recognizing kind of blade damage

parametr	frequency	component	desiner function input	Network input file
Flight speed			×	
Rotor thrust force	1ω	F_1	×	×
		F_2	×	×
	8ω	F_1	×	×
		F_2	×	
Rotor longitudinal force	1ω	F_1	×	×
		F_2	×	×
	3.25ω	F_1	×	
		F_2	×	
Shaft torsional moment	7ω	F_1	×	
		F_2	×	
Blade bending moment in plane of smaller stiffness at 0.12R location	4ω	F_1	×	
		F_2	×	×
	4.25ω	F_1	×	
		F_2	×	
Blade bending moment in plane of bigger stiffness at 0.42R location	1ω	F_1	×	×
		F_2	×	×
Hub arm in plane of rotation bending moment	1ω	F_1	×	×
		F_2	×	×
Hub arm out of rotation plane bending moment	4ω	F_1	×	
		F_2	×	
	4.25ω	F_1	×	
		F_2	×	
Out of plane blade tip deflection	1ω	F_1	×	
		F_2	×	×
Blade flap angle	1ω	F_1	×	
		F_2	×	
Blade pitch control moment	2ω	F_1	×	×
		F_2	×	

Table 3.

Input for desiner function and input files for networks including parameters measureable in flight tests conditions

parametr	frequency	component	File desiner input	Network input file						
				Damage kind	Level D1	Level D2	Level D3	Level D4	Level D5	Level D6
Flight speed			×	×	×	×	×	×	×	×
Shaft torsional moment	0		×	×	×		×	×		×
	1ω	F_1	×	×		×	×	×	×	×
		F_2	×	×	×	×	×	×	×	
	4ω	F_1	×	×	×		×	×	×	×
		F_2	×	×	×	×	×	×	×	×
Blade bending moment in plane of smaller stiffness at 0.12R location	0		×	×	×		×	×	×	×
	1ω	F_1	×	×	×	×		×	×	×
		F_2	×	×	×		×	×	×	×
	3ω	F_1	×	×	×	×	×	×	×	×
		F_2	×	×	×			×	×	×
Blade bending moment in plane of bigger stiffness at 0.42R location	0		×	×	×				×	×
	1ω	F_1	×	×	×	×	×	×		×
		F_2	×	×	×	×		×	×	×
	3ω	F_1	×	×	×			×	×	×
		F_2	×	×	×	×	×	×	×	×
Hub arm in plane of rotation bending moment	0		×	×	×	×	×	×	×	×
	1ω	F_1	×	×	×		×	×	×	×
		F_2	×	×	×	×	×	×	×	×
Hub arm out of rotation plane bending moment	0		×	×	×	×	×	×	×	×
	1ω	F_1	×	×	×	×	×		×	×
		F_2	×	×	×	×		×		×
Blade lag angle	0		×	×	×		×	×	×	×
Blade flap angle	0		×	×	×	×	×		×	×
Blade pitch control moment	0		×	×	×	×	×	×	×	×
	1ω	F_1	×	×	×				×	×
		F_2	×	×	×		×	×	×	×

Table 4.

Data of the networks for blade faults detecting (input consists of parameters measureable in flight tests conditions)

	network			Quality factor for file		
	task	type	structure	learning	validation	testing
kind of defect recognition	classifying	MLP	27:27-21-6:1	0.9570	0.9655	0.9485
estimating D1 defect level	regression	linear	26:26-1:1	0.00505	0.00499	0.00486
estimating D2 defect level	regression	MLP	16:16-7-1:1	0.00921	0.00947	0.00919
estimating D3 defect level	regression	MLP	20:20-8-1:1	0.01250	0.01209	0.01288
estimating D4 defect level	regression	MLP	24:24-6-1:1	0.00859	0.00793	0.00955
estimating D5 defect level	regression	MLP	24:24-7-1:1	0.02467	0.02235	0.02738
estimating D6 defect level	regression	linear	26:26-1:1	0.05146	0.05549	0.05108

MLP – multilayer perceptron

Table 5.

Neural network results of blade defects recognition for learning file

Defect	D1	D2	D3	D4	D5	D6	total
Number of events	577	537	571	553	520	548	3306
Correct recognized	564	511	560	548	517	464	3164
False recognized	13	26	11	5	3	84	142

Table 6.

Neural network results of blade defects recognition for validation file

Defect	D1	D2	D3	D4	D5	D6	total
Number of events	272	291	249	259	306	276	1653
Correct recognized	264	279	245	257	306	245	1596
False recognized	8	12	4	2	0	31	57

Table 7.

Neural network results of blade defects recognition for testing file

Defect	D1	D2	D3	D4	D5	D6	total
Number of events	262	272	280	288	274	276	1652
Correct recognized	256	254	273	282	271	231	1567
False recognized	6	18	7	6	3	45	85

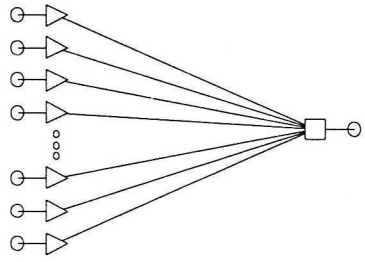

Fig. 16. Scheme of linear network 26:26-1:1 estimating the level of D1 blade defect

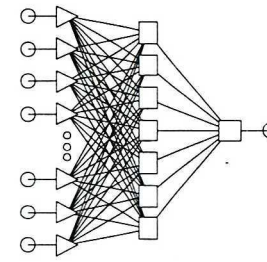

Fig. 17. Scheme of MLP multilayer perceptron network 16:16-7-1:1 estimating the level of D2 blade defect

The neural networks of regression task were trained using the same designer function input file as for the classifying network training. For the regression network, the quality network is defined as a quotient of two standard deviations: deviation of network output mistakes made for estimated values of the result parameter and deviation for output parameter values inserted into data for training. It is assumed that neural network well fulfills the regression task if standard deviations ratio reaches the value lower than *0.1* [7]. As an example, the scheme of linear network for estimating the level of D1 fault is shown in Fig. 16 and the feedforward MLP network for level of D2 fault is shown in Fig. 17.

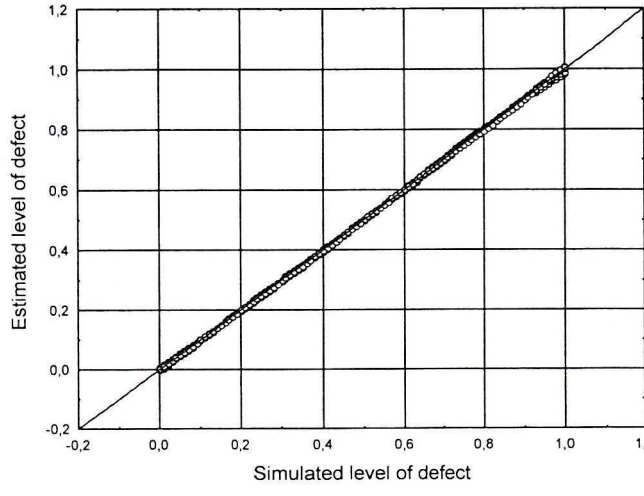

Fig. 18. Scatter plot of the simulated and estimated levels of the lag damper defects (D4)

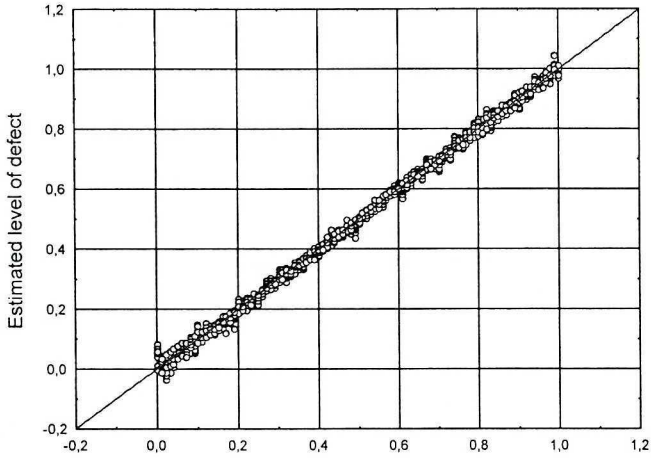

Fig. 19. Scatter plot of the simulated and estimated levels of defects (D6) – pitch control stiffness decrease

For all defects but fault D6 – decrease pitch link stiffness, the quality factors for networks estimating the development level of defects were lower than *0.027*. The quality factor for network estimating the level of D6 fault reached the value of *0.0555* (table 4). The output results for neural networks estimating the development of blade damper damage (Fig. 18) and the development of blade pitch link stiffness defect (Fig. 19) are presented as scatter plots for simulated and estimated level faults.

It should be expressed that good results obtained in applying neural networks for detecting blade faults are connected with usage in training procedure the computed data. The rotor loads calculation method assumes some simplifications in comparison with real flight conditions. In the simulation model, all blades but one have ideally the same properties The lack of air turbulence was also assumed. Fast Fourier transformation was applied to blade parameters of the simulation results for steady flight conditions. The disturbances occurring in helicopter flight can affect neural networks resulting in an increased level of the false damage recognition. Despite those minor factors, it seems that neural networks could be applied for detecting blade faults due to the changes of blade properties during helicopter life time.

5. Conclusions

The trained neural networks make it possible to correctly recognize blade defects using as input data the blade loads, the hub arm loads and the blade motion components measurable in helicopter flight conditions. Processors with an implemented code of the neural networks could provide data useful

for helicopter health monitoring system. Neural network results that detect rotor faults at low development level could increase safety of helicopter flights.

Manuscript received by Editorial Board, November 05, 2004;
final version, February 20, 2005.

REFERENCES

[1] Haas D. J., Milano J., Flitter L.: Prediction of helicopter component loads using neural networks. Journal of American Helicopter Society, Vol. 40, No. 1, pp. 72 ÷ 82, 1995.
[2] Ganguli R., Chopra I., Haas D. J.: Formulation of a helicopter rotor system damage detection methodology. Journal of American Helicopter Society, Vol. 41, No. 4, pp. 302 ÷ 312, 1996.
[3] Ganguli R., Chopra I., Haas D. J.: Detection of helicopter rotor system simulated faults using neural networks. Journal of American Helicopter Society, Vol. 42, No. 2, pp. 161 ÷ 171, 1997.
[4] Stanisławski J.: Influence of simulated blade damages on the helicopter rotor loads level. Transactions of the Institute of Aviation, No. 168–169, pp. 51 ÷ 58, 2002.
[5] Stanisławski J., Kornacki R.: Application of neural network for damage detection of helicopter rotor blade. Theoretical and applied Mechanics, 2002.
[6] Tarzanin F. J.: Prediction of control loads due to blade stall. Journal of American Helicopter Society, Vol. 17, No. 2, pp. 33 ÷ 46, 1972.
[7] STATISTICA Neural Networks. StatSoft Polska, 2001.

Zastosowanie sieci neuronowych do wykrywania uszkodzeń wirnika śmigłowca

Streszczenie

Przedstawiono możliwości zastosowania sieci neuronowych do rozpoznawania usterek łopat wirnika nośnego śmigłowca. Do treningu sieci neuronowych wykorzystano obliczeniowe dane uwzględniające zmianę obciążeń łopat i głowicy przy symulowanych uszkodzeniach. W modelu fizycznym łopaty wirnika reprezentowały osie sprężyste z dołączonym układem mas skupionych. Uszkodzenia wirnika symulowano poprzez zmianę wybranych własności aerodynamicznych, masowych lub sztywnościowych łopat.